Supporting Information

Ion-Cage Interpretation for the Structural and Dynamic Changes of Ionic Liquids under an External Electric Field

Rui Shi and Yanting Wang*

State Key Laboratory of Theoretical Physics, Institute of Theoretical Physics, Chinese Academy of Sciences, 55 East Zhongguancun Road, Beijing 100190, China

*Phone: +86 10-62648749. E-mail: wangyt@itp.ac.cn.

Contents

A. Convergence of potential energy and self-diffusion coefficient

Because the coarse-grained (CG) model has fewer number of degrees of freedom, it typically has much softer interaction potentials than the all-atom case, thereby allows a faster dynamics. Due to the sluggish nature of ILs, with an all-atom model, 2-4 ns simulation time might not be sufficient for studying the dynamic properties of ILs. However, with our EF-CG model, because of the significantly accelerated dynamics, a 2 ns CG simulation at T = 400 K is long enough for [EMIm][NO3], as justified by the following results.

In Figure S1(a), we plot the potential energies as a function of time from three 2-4 ns *NVT* trajectories at different electric fields. It can be seen that the potential energies converge very quickly. The potential value drops at the beginning because the initial configurations of these *NVT* runs are sampled from a high temperature (T = 2000 K) trajectory. In Figure S1(b), we show the self-diffusion coefficients as a function of simulation length t. It can be seen that the self-diffusion coefficients fluctuate slightly and do not change much in a wide range of simulation lengths from 500 ps to 40 ns and hence a 2 ns trajectory is long enough for studying the dynamics. Moreover, since an ensemble of many independent short trajectories can explore the phase space more sufficiently than a single long trajectory, we simulated an ensemble of 20 independent trajectories to ensure a better statistics.

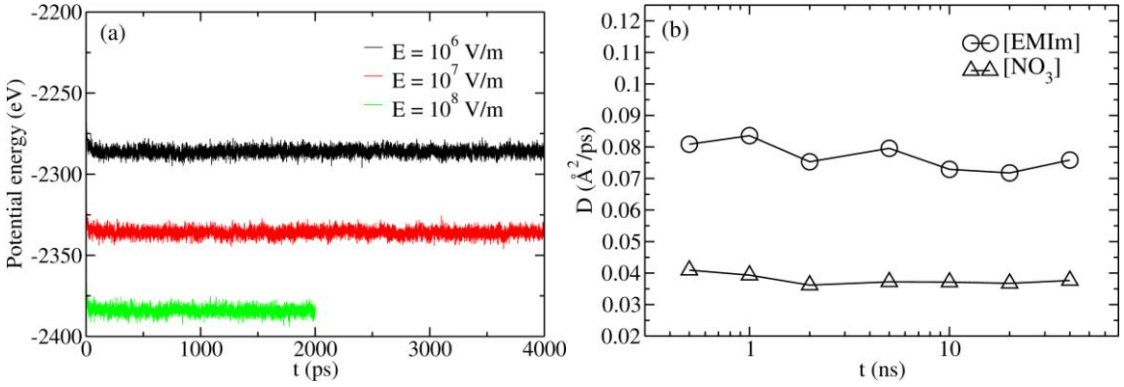

Figure S1. (a) Potential energies as a function of time. The values for 10^6 and 10^7 V/m are offset by +100 and +50 eV, respectively. (b) Self-diffusion coefficients as a function of simulation length.

B. Thermostat in nonequilibrium steady states

Special attention should be paid when applying a thermostat in a nonequilibrium steady state, since currently most thermostats are developed for equilibrium states. When simulating an equilibrium state, temperature is defined as the average kinetic energy of particles.[1] In nonequilibrium steady states, however, the equilibrium temperature allows the drift motion to contribute an extra translational energy to the total kinetic energy and thus overestimates the thermal motion of the system. Therefore, when the drift motion is large, an artificial "freezing" effect is introduced to the simulation for a nonequilibrium steady state.[2] Because until now the temperature for nonequilibrium states is still not well-defined,[3] the thermostats defined for equilibrium states are practically used for nonequilibrium molecular dynamics (MD) simulations. Fortunately, as studied by Delhommelle et al.,[2, 4] the artificial "freezing" effect

becomes non-negligible only at a very strong external electric field, and all the properties calculated with different thermostats converge to the same value when the electric field is weaker than 10^9 V/m and the drift energy is negligible compared with the thermal energy.

In this work, our calculations indicate that, at $E < 4 \times 10^8$ V/m, the drift energy is less than 0.5 % of the kinetic energy and thus the artificial effect in this region is negligible; even with the strongest electric field $E = 10^9$ V/m in our MD simulations, the drift energy is only 12 % of the total kinetic energy. Therefore, the "freezing" effect that slows down the dynamics of ions slightly underestimates the mobility and self-diffusion only when the electric field reaches 10^9 V/m. Nevertheless, since our present results reveal that the dynamic properties gradually increase with electric field in the strong field region, the underestimation due to the freezing effect does not do harm to our qualitative conclusions.

C. Challenges in determining the drift velocity

Due to the strong intrinsic electric field[5] and the sluggish nature of ionic liquids (ILs), the response of ILs to a weak or moderate external electric field is quite feeble and inconspicuous. As a result, characterizing the effect of an electric field on the structure and dynamics of ILs are very difficult in both experiments and simulations. One of the most important quantities for ILs in a nonequilibrium state is the ion drift velocity characterizing the charge transport in the system. Under an electric field E, the drift velocity v of an ion with a charge ze can be calculated from the conductivity σ by the following equation,[6]

$$J = \sigma E = zFcv \tag{S1}$$

where J is the current density, F is the Faraday constant, and c is the molar concentration. Take 1-ethyl-3-methylimidazolium tetrafluoroborate ([EMIm][BF4]) as an example. The conductivity of [EMIm][BF4] is 1.31 S/m at 298 K.[7] If we assume that cations and anions have the same drift velocity, under a weak electric field of 100 V/m, the ion drift velocity is estimated to be around 10^{-7} m/s, which is not detectable both in present experiment[8] and molecular dynamics simulation (10^{-7} m/s is equal to a 10^{-5} nm displacement in a 100 ns MD simulation).

On the other hand, the thermal velocity can be estimated by the following equation

$$v_{\text{thermal}} = \sqrt{3k_{\text{B}}TN_{\text{A}}/M} \tag{S2}$$

where k_{B} is the Boltzmann constant, T is the temperature, N_{A} is the Avogadro constant, and M is the molar mass. For [EMIm][BF_4], the thermal velocity is about 190 m/s at 298 K. In the case of [EMIm][NO_3] at 400 K, the thermal velocity is around 240 m/s. Clearly, the thermal velocity is usually several orders of magnitude larger than the ion drift velocity at weak electric fields, and thus the small drift velocity is submerged in the large thermal velocity. Therefore, the determination of the drift velocity in ILs is very challenging for both experiments and simulations.

D. Density

With the system size determined from a constant *NPT* simulation, the bulk density of [EMIm][NO3] was calculated at different electric fields. As shown in Figure S2, the system density apparently decreases with increasing electric field in the strong field region, but shows no obvious changes under moderate electric fields. This is consistent with the radial distribution function results shown in the main text indicating that the system expands when a strong electric field is applied. This field-induced expansion seems to be quite general in ILs, since it is independent of alkyl chain length, as presented by our previous work.[9]

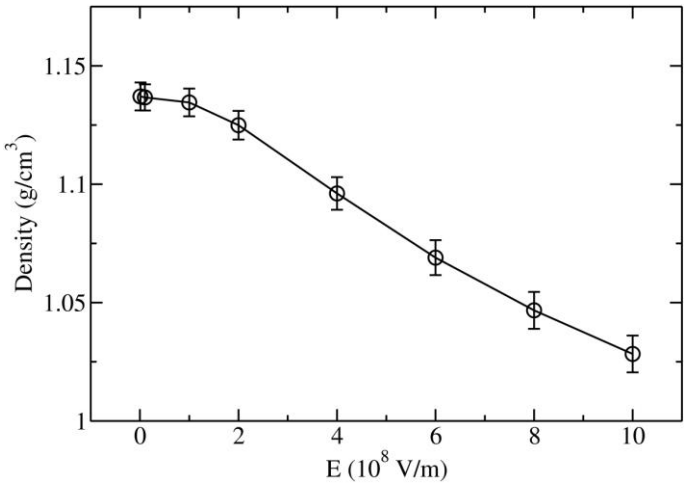

Figure S2. Density of [EMIm][NO_3] as a function of the field strength *E* at *P* = 1 atm and *T* = 400 K.

E. Gaussian fit for ion position distribution in ion cage

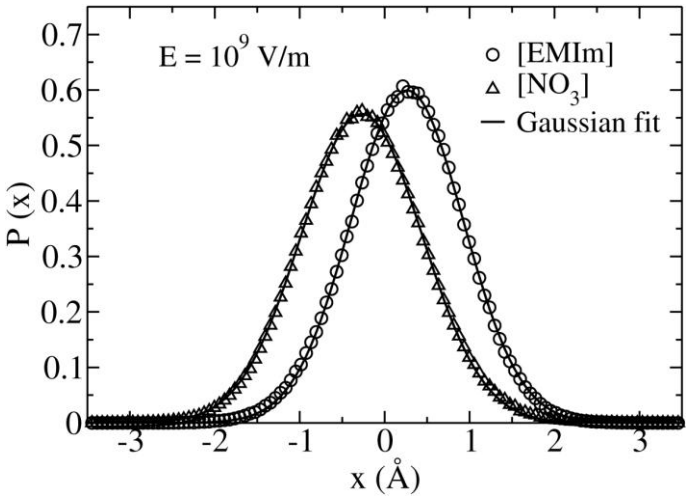

Figure S3. Gaussian fits to the one-dimensional ion position distributions with respect to the center of mass of the ion cage along the *X* axis at an electric field of 10^9 V/m.

The one-dimensional ion position distributions with respect to the center of mass of the ion cage along the *X* axis (external field direction) at an electric field of 10^9 V/m were fitted to a Gaussian form,

$$P(x) = A\exp\left(-\frac{(x-B)^2}{2C^2}\right) \quad \text{(S3)}$$

As shown in Figure S3, the distributions have a perfect Gaussian form with the coefficient of determination R^2 = 0.9999 for both cation and anion at $E = 10^9$ V/m. The perfect Gaussian forms (with the coefficient of determination R^2 = 0.9999) were also found for the distributions in all the *X*, *Y*, and *Z* directions and at all the electric fields investigated in the present work (Data are not shown).

F. Anisotropy of ion cage

To further quantify the anisotropy of effective cage potential, the regular sphere-averaged radial distribution functions (RDFs) were decomposed into three angle-resolved components. Figure S4 shows the angle-resolved cation-anion RDFs falling into the cones of angle 45 ° around the *X* (external field direction), *Y*, and *Z* axes (see the inset in Figure S4(a)) at different electric fields. Clearly, the ions in the first coordination shell tend to distribute more in the *Y* and *Z* directions than in the *X* direction, as presented by the lower first peak along the *X* axis. The anisotropic distribution is enhanced as the electric field increases. This indicates that a strong electric field deforms the ion cage and leads to an anisotropic cage potential well.

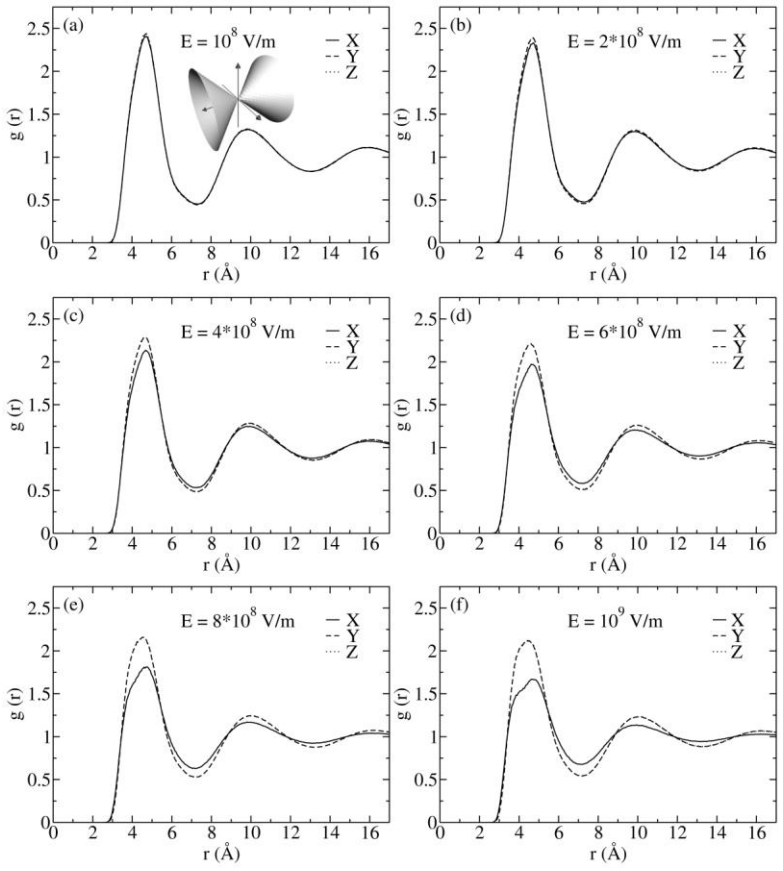

Figure S4. Angle-resolved radial distribution functions (RDFs) between the center of mass of cations and anions at different strengths of external electric fields. "X", "Y", and "Z" denote the RDFs falling into the cones of angle 45° around the *X*, *Y*, and *Z* axes, respectively (See the schematic in the inset of (a)).

G. Orientation of cation

Besides ion cage structure, the orientation of ions might also affect the dynamic properties such as mobility and diffusion of ILs by providing ion transport pathways formed by the alignment of ions along the electric field.[10] The distribution of the angle between the *X* axis and the vector pointing from site E to site B of cation is shown in Figure S5. Clearly, the orientation of cations is totally random at moderate electric fields, and a preferential direction of cation being parallel to the electric field was observed when the electric field is stronger than 10^7 V/m. Similar to the ion cage structure, the cationic orientation has noticeable changes only at strong electric fields.

Besides the applied electric field, the orientational ordering in ILs also enhances with increasing alkyl chain length. The orientational ordering of [EMIm][NO_3] increases with the electric field strength, but is still much weaker than the ILs with longer alkyl chains at the same electric field, as shown in our previous work.[9] Those observations can be explained by the fact that the charged cationic head groups are pulled forward by the applied electric field, leaving behind the nonpolar tails due to the friction drags. Because a longer cationic tail experiences a larger frictional force, the long-chain IL system exhibits stronger orientational ordering.

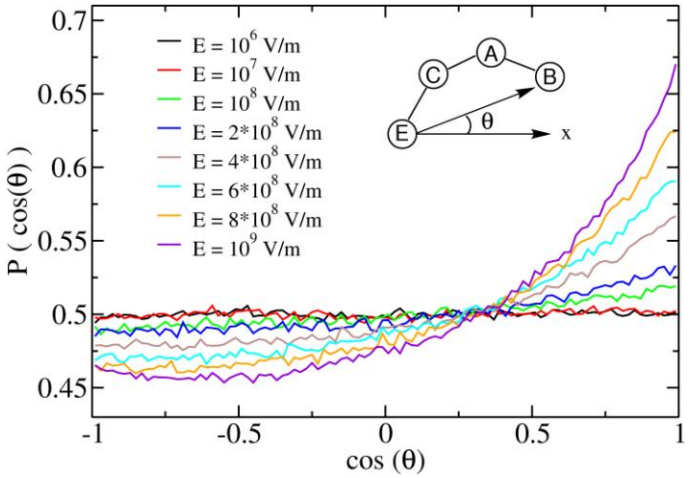

Figure S5. Distributions of the angles between the *X* axis and the vector connecting site E and site B of cation at different strengths of external electric fields.

H. Relative mean-square displacement

In equilibrium, the self-diffusion coefficient *D* in three dimensions can be calculated from the mean-square displacement (MSD) $\left\langle \Delta r^2(t) \right\rangle$ by using the Einstein expression

$$\left\langle \Delta r^2(t) \right\rangle = 6Dt \tag{S4}$$

which denotes that, for a diffusive motion, the MSD increases linearly with time *t*. However, when the IL system is driven out of equilibrium by an external electric field, the MSD does not exhibit a normal diffusive behavior, because the drift motion will also contribute to the overall MSD. To obtain the

self-diffusion coefficient in a nonequilibrium steady state, the relative MSD in one-dimension along the field direction is defined to deduct the drift contribution from the overall MSD as

$$\left\langle x^2(t)\right\rangle - \left\langle x(t)\right\rangle^2 = \left\langle \left(x(t) - \left\langle x(t)\right\rangle\right)^2 \right\rangle = 2D_x t \tag{S5}$$

The one-dimensional relative MSDs as a function of time at different electric fields are shown in Figure S6. The relative MSD exhibits good linear behavior at all the electric fields studied in the present work (data at $E < 10^6$ V/m are not shown). According to eq S5, the effective self-diffusion coefficient can be obtained by a linear fit to the relative MSD.

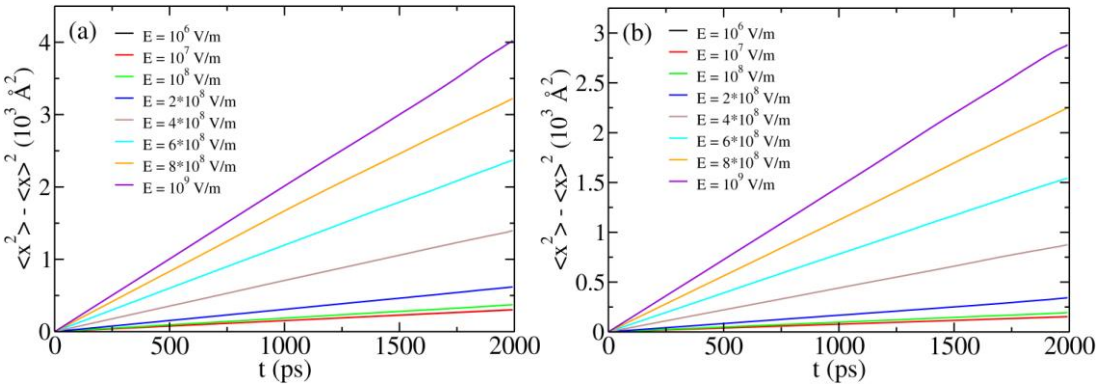

Figure S6. One-dimensional relative mean-square displacements as a function of time at different strengths of external electric fields for cations (a) and anions (b) along the *X* axis.

I. Activation energy

To estimate the activation energy in the system, we fitted the self-diffusion coefficients $D(E)$ to the Arrhenius law,

$$D(E) = D_0 \exp\left[-\frac{Q_a(E)}{k_B T}\right] \tag{S6}$$

where k_B is the Boltzmann constant, T is the temperature, D_0 is the pre-exponential factor, and $Q_a(E)$ is the activation energy at an electric field E. By assuming that the pre-exponential factor is insensitive to the external electric field, the relative activation energy can be obtain by the expression

$$\Delta Q_a(E) = Q_a(E) - Q_a(E_0) = k_B T \ln \frac{D(E_0)}{D(E)} \tag{S7}$$

where $Q_a(E_0)$ and $D(E_0)$ are the activation energy and self-diffusion coefficient in the absence of external electric field. The relative activation energies at different directions are plotted as a function of electric field strength in Figure S7.

It can be seen that, at strong electric fields, the relative activation energy decreases apparently with electric field strength for both cations and anions. Moreover, the effective potential well becomes anisotropic, with a lower energy barrier along the electric field than those perpendicular to the field. The

inset in Figure S7 plots the relative activation energies at electric fields ranging from 10 to 10^7 V/m. Clearly, the relative activation energy remains almost constant at weak and moderate fields, which again supports our previous results that a weak or moderate field can hardly change the structural and dynamic properties of ILs in an influential way.

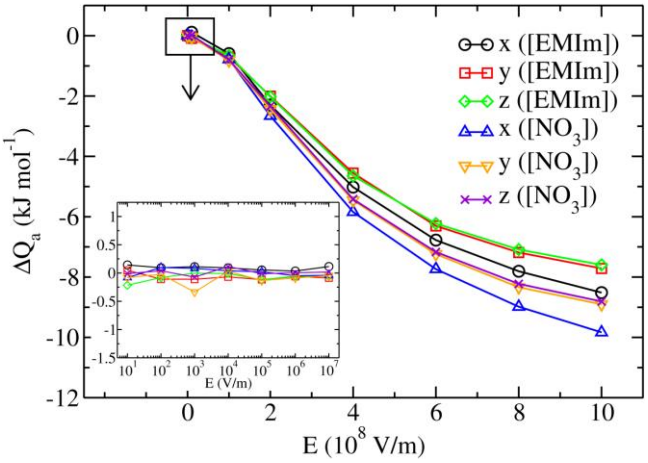

Figure S7. Relative activation energies at different directions as a function of electric field strength. Inset: magnified plot for 10 - 10^7 V/m.

J. Einstein relation

Table S1. Overall scaled mobilities and self-diffusion coefficients of the whole system at different electric fields.

Moderate electric fields			Strong electric fields		
E (V/m)	$u'_+ + u'_-$ (Å^2/ps)	$D_+ + D_-$ (Å^2/ps)	E (V/m)	$u'_+ + u'_-$ (Å^2/ps)	$D_+ + D_-$ (Å^2/ps)
10^6	0.07 ±0.12	0.11 ±0.004	10^8	0.13 ±0.002	0.14 ±0.007
2×10^6	0.11 ±0.06	0.11 ±0.005	2×10^8	0.17 ±0.002	0.22 ±0.01
4×10^6	0.12 ±0.03	0.11 ±0.005	4×10^8	0.29 ±0.001	0.52 ±0.02
6×10^6	0.12 ±0.03	0.11 ±0.004	6×10^8	0.40 ±0.001	0.87 ±0.04
8×10^6	0.12 ±0.02	0.11 ±0.004	8×10^8	0.49 ±0.001	1.18 ±0.05
10^7	0.12 ±0.02	0.11 ±0.004	10^9	0.56 ±0.001	1.43 ±0.05

Table S1 lists the overall scaled mobility and overall self-diffusion coefficient of the whole system at different electric fields. It seems that, at moderate fields, the scaled mobility approximately equals to the self-diffusion coefficient within the statistical error. However, at strong electric field, the Einstein relation of the whole system apparently breaks down.

K. Structure and dynamics under weak electric fields

In this section, the structural and dynamic analyses were performed in the absence and in presence of a weak electric field (0 - 10^6 V/m). As shown in Figures S8, S9, and S10, the radial distribution

functions, ion position distributions in the cage, and the cation orientation all show no detectable changes under weak electric fields. Accordingly, as listed in Table S2, the density and effective cage potential strength keep constant within the statistical error. Moreover, the ion cage dynamics and effective self-diffusion coefficient also remain unchanged, as presented in Figure S11 and Table S3. These results indicate that a weak electric field can hardly alter the structural and dynamic properties of ILs in an influential way.

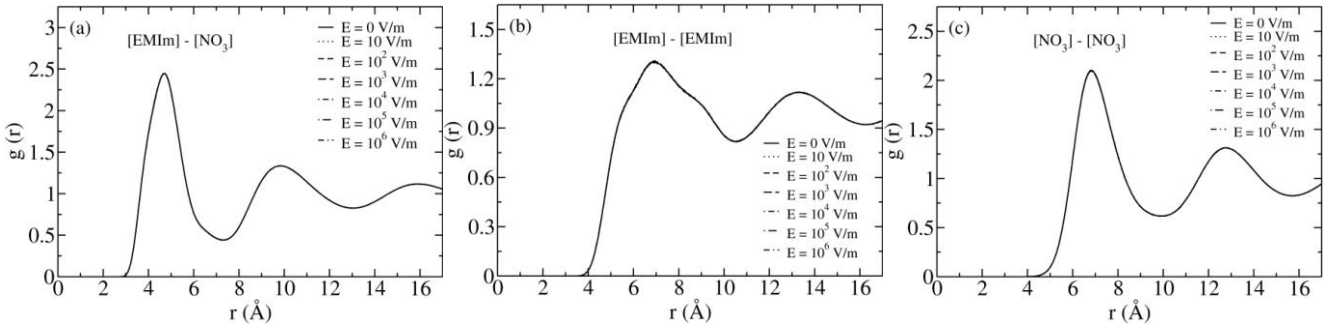

Figure S8. Radial distribution functions between the center of mass of cations and anions (a), cations and cations (b), and anions and anions (c) at electric fields ranging from 0 – 10^6 V/m. The curves exactly overlap with each other.

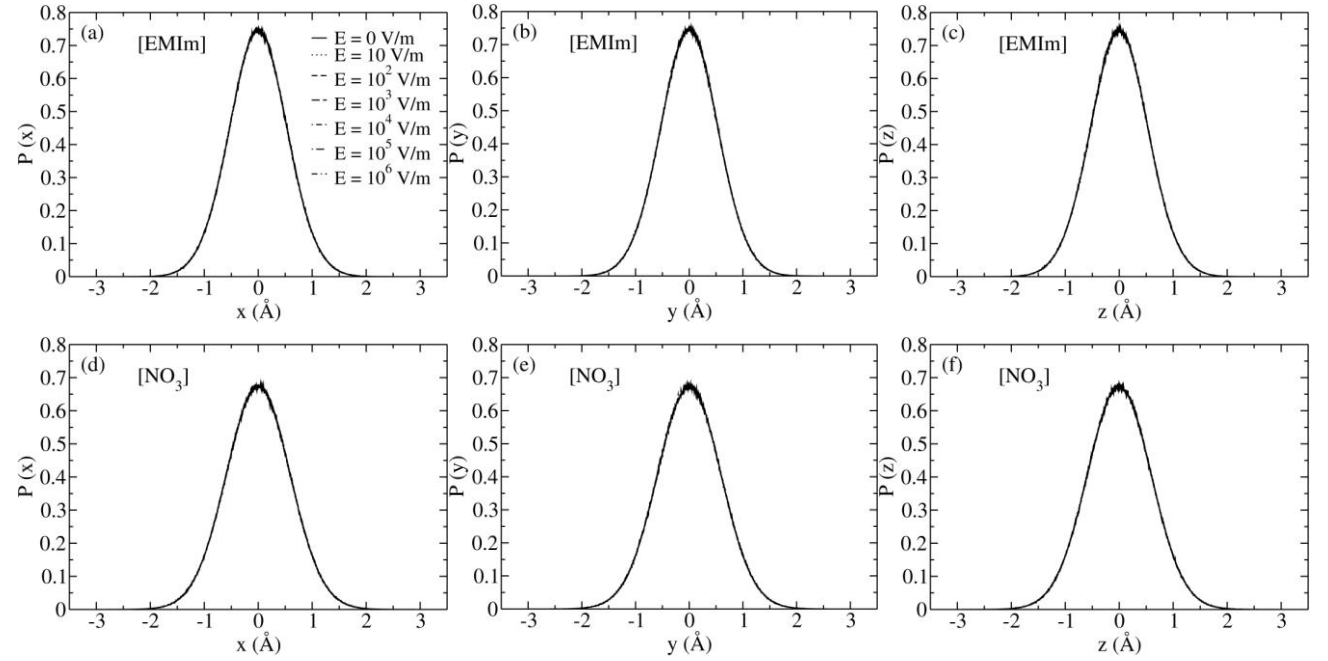

Figure S9. One-dimensional ion position distributions with respect to the center of mass of the ion cage along the *X*, *Y*, and *Z* directions at electric fields ranging from 0 – 10^6 V/m. The curves exactly overlap with each other.

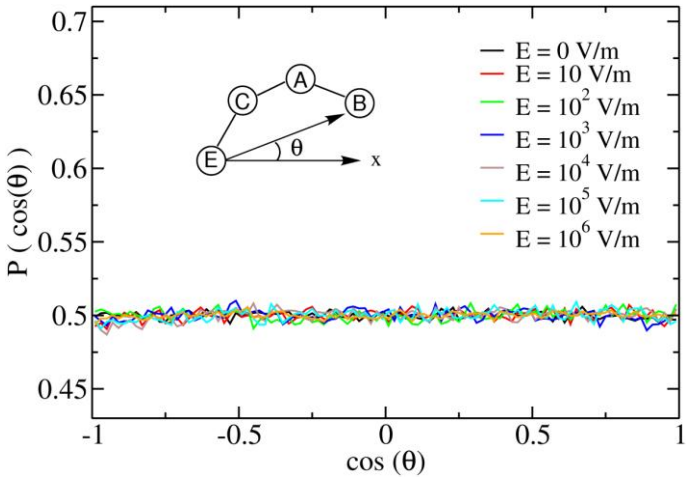

Figure S10. Distributions of the angle between the external field direction and the vector connecting site E and site B of cation at electric fields ranging from 0 – 10^6 V/m.

Table S2. Density and cage potential strengths along the *X*, *Y*, and *Z* directions at external electric fields ranging from 0 – 10^6 V/m.

E (V/m)	Density (g/cm^3)	U_0 (kJ mol^{-1} $Å^{-2}$)					
		EMIm			NO_3		
		X	*Y*	*Z*	*X*	*Y*	*Z*
0	1.137	5.80	5.78	5.78	4.73	4.72	4.74
10	1.136	5.78	5.77	5.80	4.74	4.71	4.74
10^2	1.137	5.79	5.79	5.78	4.73	4.74	4.73
10^3	1.137	5.79	5.78	5.79	4.74	4.74	4.73
10^4	1.137	5.79	5.77	5.77	4.74	4.74	4.73
10^5	1.137	5.79	5.78	5.77	4.74	4.73	4.74
10^6	1.137	5.79[a]	5.78	5.79	4.74	4.73	4.73

[a] From 20 independent trajectories at $E = 10^6$ V/m. The standard deviations of U_0 are within 0.02 kJ mol^{-1} $Å^{-2}$ for both cation and anion in all directions.

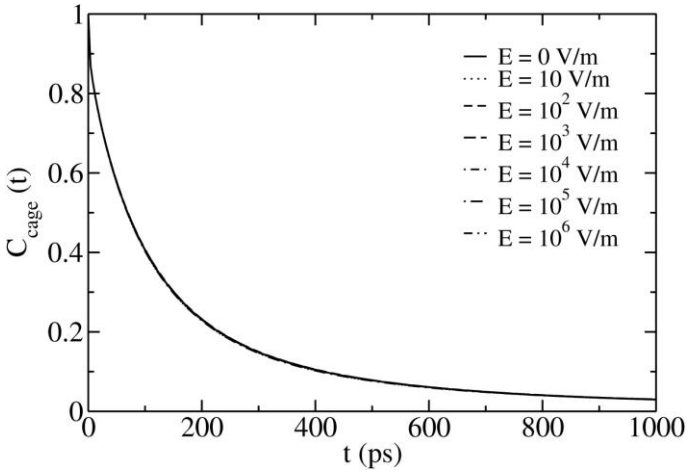

Figure S11. Time correlation functions of ion cage dynamics at external electric fields ranging from 0 – 10^6 V/m. The curves exactly overlap with each other.

Table S3. Effective Self-Diffusion Coefficient of [EMIm][NO_3] at external electric fields ranging from 0 – 10^6 V/m.

E (V/m)	D_{eff} (Å^2 ps^{-1})	
	EMIm	NO3
0	0.076	0.038
10	0.074	0.040
10^2	0.076	0.039
10^3	0.077	0.040
10^4	0.073	0.037
10^5	0.077	0.038
10^6	0.076[a]	0.038

[a] From 20 independent trajectories at E = 10^6 V/m. The standard deviations are 0.002 and 0.001 Å^2 ps^{-1} for cation and anion, respectively.

L. Conductivity

The out-of-equilibrium conductivity can be calculated from the ion mobility by using the equation[6]

$$\sigma = ne\left(z_+u_+ + z_-u_-\right) \tag{S8}$$

where n is the IL number density, e is the proton charge, z_+ and z_- are the ionic charges, and u_+ and u_- are the mobilities of cation and anion, respectively. For comparison, the near-equilibrium conductivity was calculated from an equilibrium trajectory by using the Green-Kubo relation[4, 6]

$$\sigma = \frac{V}{3k_B T}\int_0^{\infty} \langle j(t)\, j(0) \rangle \mathrm{d}t \tag{S9}$$

where V is the volume of the system, k_B is the Boltzmann constant, T is the temperature, and $j(t)$ is the electric current density at time t, which can be obtained from the following equation

$$j = \frac{e}{V}\sum_{i=1}^{N} z_i v_i \tag{S10}$$

where N is the number of ions, z_i is the ionic charge of ion i, and v_i is the velocity of ion i.

The near-equilibrium conductivity of [EMIm][NO_3] was calculated from a 4-ns equilibrium trajectory by using the Green-Kubo relation. The time-dependent conductivity is shown in Figure S12. The near-equilibrium conductivity was obtained from the average value at long time.

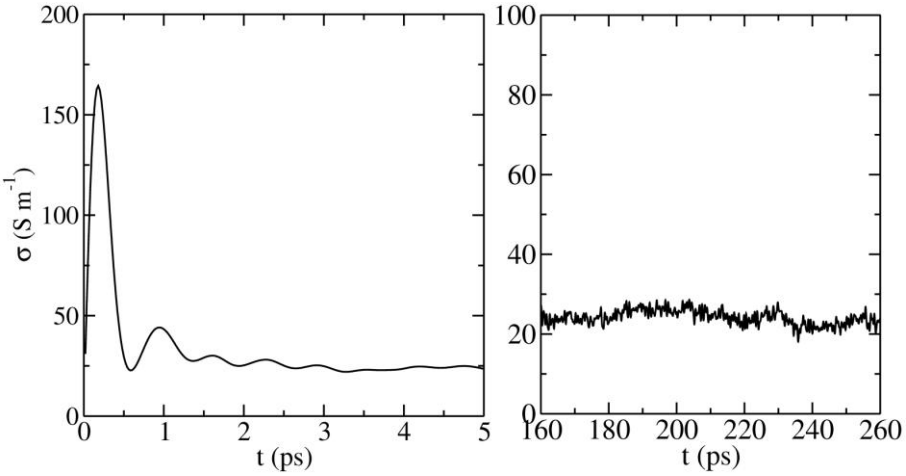

Figure S12. Time-dependent conductivity calculated by using the Green-Kubo relation. On the right panel we show the convergence of the conductivity at long time.

Moreover, to check the conductivity calculated by using the Green-Kubo relation from a 4-ns trajectory, we also calculated the conductivity from a 40-ns equilibrium trajectory by using the MSD[11-13]

$$\sigma = \frac{e^2}{k_B T V}\lim_{t\to\infty}\frac{1}{6t}\left\langle \left| z_+ R_+(t) + z_- R_-(t) \right|^2 \right\rangle \tag{S11}$$

where $R_\alpha(t)$ is the displacement of all the ions of species α at time t,

$$R_\alpha(t) = \sum_{i\in\alpha} \delta r_i(t) \tag{S12}$$

and $\delta r_i(t)$ is the displacement of ion i in time t. The conductivity was then obtained by a linear fit to the MSD in its linear region (0 - 1 ns).

Since the ion drift velocity at a weak field is too weak to be determined from our simulations, we cannot calculate the ion mobility at weak electric fields. However, by employing the MSD and

Green-Kubo equation, we can calculate the near-equilibrium conductivity of [EMIm][NO_3] and compare it with the out-of-equilibrium conductivities calculated from the mobilities at moderate electric fields. The result is plotted in Figure S13. It can be seen that the MSD and Green-Kubo relation give almost the same near-equilibrium conductivity. Moreover, the conductivity at moderate electric fields almost remains constant and approximately equals to the near-equilibrium conductivity within the statistical error. Although our calculated conductivity is several times larger than the typical experimental value of ILs due to the acceleration of the coarse-graining model, (e.g., 4.55 S/m for [EMIm][BF_4] at 373.15 K[7] and no experimental conductivity for [EMIm][NO_3] at 400 K) the trend displayed in Figure S13 again supports the assertion that a weak or moderate electric field can hardly change the dynamic properties of ILs in an influential way.

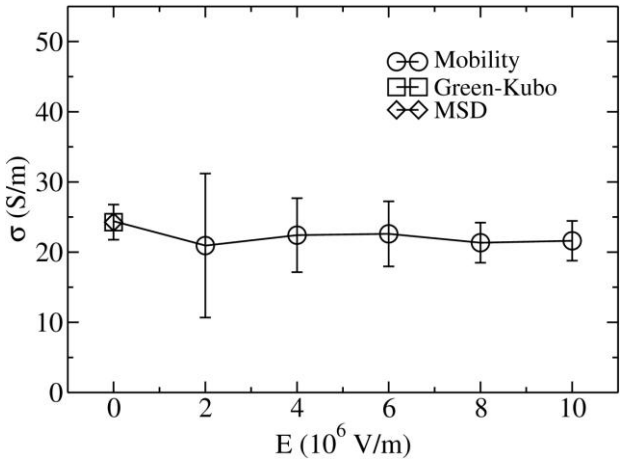

Figure S13. Conductivities calculated by using the MSD and Green-Kubo relation in equilibrium and the mobility at moderate electric fields. The error bar at E = 0 represents the standard error of conductivity calculated by using the Green-Kubo relation.

References

(1) Frenkel, D.; Smit, B., *Understanding Molecular Simulation: From Algorithms to Applications*. Academic: San Diego, 2002.

(2) Delhommelle, J. Should "Lane Formation" Occur Systematically in Driven Liquids and Colloids? *Phys. Rev. E* **2005,** *71*, 016705.

(3) Casas-Vázquez, J.; Jou, D. Temperature in Non-Equilibrium States: A Review of Open Problems and Current Proposals. *Rep. Prog. Phys.* **2003,** *66*, 1937-2023.

(4) Petravic, J.; Delhommelle, J. Conductivity of Molten Sodium Chloride and Its Supercritical Vapor in Strong dc Electric Fields. *J. Chem. Phys.* **2003,** *118*, 7477-7485.

(5) Zhang, S.; Shi, R.; Ma, X.; Lu, L.; He, Y.; Zhang, X.; Wang, Y.; Deng, Y. Intrinsic Electric Fields in Ionic Liquids Determined by Vibrational Stark Effect Spectroscopy and Molecular Dynamics Simulation. *Chem.-Eur. J.* **2012,** *18*, 11904-11908.

(6) Atkins, P.; de Paula, J., *Atkins' Physical Chemistry*. 7th ed.; Oxford University Press: Oxford, 2002.

(7) Fuller, J.; Carlin, R. T.; Osteryoung, R. A. The Room Temperature Ionic Liquid 1-Ethyl-3-methylimidazolium Tetrafluoroborate: Electrochemical Couples and Physical Properties. *J. Electrochem. Soc.* **1997,** *144*, 3881-3886.

(8) Hayamizu, K.; Aihara, Y. Correlating the Ionic Drift under Pt/Pt Electrodes for Ionic Liquids Measured by Low-Voltage Electrophoretic NMR with Chronoamperometry. *J. Phys. Chem. Lett.* **2010,** *1*, 2055-2058.

(9) Zhao, H.; Shi, R.; Wang, Y. Nanoscale Tail Aggregation in Ionic Liquids: Roles of Electrostatic and Van Der Waals Interactions. *Commun. Theor. Phys.* **2011,** *56*, 499-503.

(10) Umecky, T.; Saito, Y.; Matsumoto, H. Direct Measurements of Ionic Mobility of Ionic Liquids Using the Electric Field Applying Pulsed Gradient Spin−Echo NMR. *J. Phys. Chem. B* **2009,** *113*, 8466-8468.

(11) Castiglione, M. J.; Madden, P. A. Fluoride Ion Disorder and Clustering in Superionic PbF_2. *J. Phys.: Condens. Matter* **2001,** *13*, 9963-9983.

(12) Morgan, B.; Madden, P. A. Ion Mobilities and Microscopic Dynamics in Liquid (Li,K)Cl. *J. Chem. Phys.* **2004,** *120*, 1402-1413.

(13) Zhao, W.; Leroy, F.; Heggen, B.; Zahn, S.; Kirchner, B.; Balasubramanian, S.; Müller-Plathe, F. Are There Stable Ion-Pairs in Room-Temperature Ionic Liquids? Molecular Dynamics Simulations of 1-n-Butyl-3-methylimidazolium Hexafluorophosphate. *J. Am. Chem. Soc.* **2009,** *131*, 15825-15833.